Design and Characterization of Novel Porphyrins with Oligo(phenylethylnyl) Links of Varied Length for Dye-Sensitized Solar Cells: Synthesis and Optical, Electrochemical, and Photovoltaic Investigation

Ching-Yao Lin,*,† Chen-Fu Lo,† Liyang Luo,‡,§ Hsueh-Pei Lu,‡ Chen-Shiung Hung,§ and Eric Wei-Guang Diau*,‡

Department of Applied Chemistry, National Chi Nan University, Puli, Nantou 545, Taiwan, Department of Applied Chemistry and Institute of Molecular Science, National Chiao Tung University, Hsinchu 300, Taiwan, and Institute of Chemistry, Academia Sinica, Taipei 115, Taiwan

Received: July 30, 2008; Revised Manuscript Received: September 29, 2008

Novel zinc porphyrins with 1−4 π-conjugated phenylethylnyl (PE) units (labeled PE1−PE4) as a link of controlled length were synthesized for fundamental tests and applications as a dye-sensitized solar cell (DSSC). The UV−visible spectra of the solution samples show clear absorption patterns of the PE groups in a region 300−400 nm, consistent with results calculated with density-functional theory. Cyclic voltammograms of PE1−PE4 in tetrahydrofuran show similar electrochemical potentials for each compound. Femtosecond fluorescence up-conversion of solution samples and of porphyrin-sensitized TiO_2 films was measured with excitation at 420 or 430 nm and emission at 460, 470, 620, and 680 nm. When these porphyrins were fabricated into DSSC devices, the efficiency of power conversion of these devices decreased systematically with increasing length of the link: 2.5 ± 0.2% (PE1), 2.0 ± 0.1% (PE2), 0.78 ± 0.09% (PE3), 0.25 ± 0.02% (PE4). This great photovoltaic degradation from PE1 to PE4 is not interpretable according to the rate of electron injection independent of length; other factors, including electron transfer from the semiconductor back to the porphyrin cation or the electrolyte, must be considered to account for the observed dependence of photovoltaic performance on length.

1. Introduction

The adsorption of selected photosensitizers on nanocrystalline films, having a large surface area, of semiconductors with a wide band gap, such as titanium dioxide (TiO_2), has been an active area of research on efficient dye-sensitized solar cells (DSSC).[1] The covalent attachment of electrochemically and photochemically active chromophores to semiconductor surfaces is an important step toward the development of such devices. Because of their efficacy in this respect, Ru^{II} polypyridyl complexes adsorbed on TiO_2 nanocrystalline films have proved promising systems. Among Ru^{II} polypyridyl complexes, the so-called N3 dye, $Ru^{II}(dcbpyH_2)_2(NCS)_2$, is the most efficient photosensitizer known.[2] This N3 dye exhibits an efficiency of incident conversion of photons to electrons (IPCE) as great as 85% in the region 400−800 nm and an overall efficiency (η) 11% of power conversion.[3] Porphyrins have become prospective photosensitizers[4] because of the vital roles of porphyrin derivatives in photosynthesis, their strong absorption in the visible region, and the ease of adjusting their chemical structures (hence their electrochemical and photochemical properties) for light harvesting. Adsorbing porphyrins with modified structures onto TiO_2 nanocrystalline films thus provides an opportunity to improve DSSC applications. The best performance of a porphyrin-sensitized SC has attained $\eta = 7.1\%$.[4d]

Several factors are considered important when seeking or designing an efficient photosensitizer. The appropriate sensitizers should have these properties: the ability to adsorb strongly on the surface of a semiconductor, absorption of light in the visible and NIR region for efficient light harvesting, an excited-state reduction potential negative enough for efficient electron injection, a ground-state reduction potential positive enough for efficient regeneration of the dye, and a small reorganizational energy for efficient excited- and ground-state electrochemical processes.[5] The relation between the orientation of attached porphyrins with respect to TiO_2 nanocrystalline surfaces and the cell performance has been investigated.[4b,6] For porphyrins,[4,6] an efficient injection of electrons from the photosensitizer into a semiconductor is considered a crucial factor in developing an efficient DSSC. Apart from the effect of cosensitization,[7] the performance of a cell can be improved through appropriate modification of a dye structure with a selected link.

We reported[8] the fundamental properties of a novel porphyrin in solution and adsorbed on TiO_2 nanocrystalline films. In our design, 10,20-biphenylporphinato zinc(II) (ZnBPP) served as a light-harvesting center and a carboxylic acid as an anchoring group. To control the distance between the porphyrin and the anchoring group, we utilized a phenylethylnyl (PE) unit as a bridging moiety to connect a meso position of ZnBPP and the carboxylic acid end. We chose ZnBPP because of its ease of synthesis, the stability of zinc porphyrins against irradiation, and the efficiency of zinc porphyrins that is superior to that of copper and free-base porphyrins.[4b] 4-Carboxylic acid groups were used to ensure efficient adsorption on TiO_2 surfaces and to promote electronic coupling between the donor levels of the excited porphyrins and the acceptor levels of TiO_2.[6] PE units were employed to control the distance because of their rigidity, their linear structure, and the possible π interactions between the porphyrin core and the anchoring end.[9] Porphyrins with an

* To whom correspondence should be addressed. E-mail: cyl@ncnu.edu.tw (C.-Y.L.); diau@mail.nctu.edu.tw (E.W.-G.D.).
† National Chi Nan University.
‡ National Chiao Tung University.
§ Academia Sinica.

10.1021/jp806777r CCC: $40.75
Published on Web 12/22/2008

ethynyl motif were employed for photonic and electrochemical tests on multichromophore arrays.[10]

PE units as spacers have been reported for other systems.[10b,11] For example, seeking to use porphyrins as molecular photonic materials, Lindsey and co-workers investigated several multiporphyrin arrays to understand their energy-transfer phenomena;[12] in their design, monomeric chromophores were linked with phenyl-ethynyl-phenyl bridging groups to create weak interactions between the chromophores and to preserve the characteristics of each chromophore.[10b,c] Piotrowiak et al. reported "tripod" Ru^{II} complexes with PE groups as rigid links to connect the sensitizers and TiO_2;[11] these sensitizers consisted of a tripod-shaped base with three COOR groups to attach to TiO_2 nanocrystalline surfaces, a rigid (4-ethynyl)phenylethyne spacer, and a Ru^{II} complex as a chromophoric center. The base design provides a stable and well-defined orientation of the sensitizers with respect to the nanoparticulate surfaces, whereas the rigidity of the (4-ethynyl)phenylethyne spacer ensures control of the distance between the light-harvesting centers and the TiO_2 surfaces.

To investigate the interfacial electron transfer and for DSSC applications with a similar design, we have prepared novel porphyrins: 5-(4-carboxy-phenylethynyl)-10,20-biphenylporphinato zinc(II), 5-[4-(4-carboxy-phenylethynyl)-phenylethynyl]-10,20-biphenylporphinato zinc(II), 5-{4-[4-(4-carboxy-phenylethynyl)-phenylethynyl]-phenylethynyl}-10,20-biphenylporphinato zinc(II), and 5-(4-{4-[4-(4-carboxy-phenylethynyl)-phenylethynyl]-phenylethynyl}-phenylethynyl)-10,20-biphenylporphinato zinc(II), abbreviated PE1, PE2, PE3, and PE4, respectively. As shown in Chart 1, these porphyrins share the same light-harvesting unit (ZnBPP) with rigid, linear, edgewise, and fully conjugated substituents of varied length.

When we fabricated DSSC devices using PE1−PE4 as photosensitizers, the cell performance of the devices exhibited a systematic dependence on length according to which the DSSC with a long link (PE4) performed much less effectively than the DSSC with a short link (PE1). To understand the interfacial electron-transfer dynamics that govern the photovoltaic performance of the system dependent on length, we conducted femtosecond measurements, and we report here the spectral and electrochemical properties and the fluorescence decay of PE1−PE4 in solution and on TiO_2 nanocrystalline films.

CHART 1: Molecular Structures of ZnBPP and PE1−PE4 with the Distance between the Porphyrin Core and the Anchoring Group Calculated with Density Functional Theory (DFT)

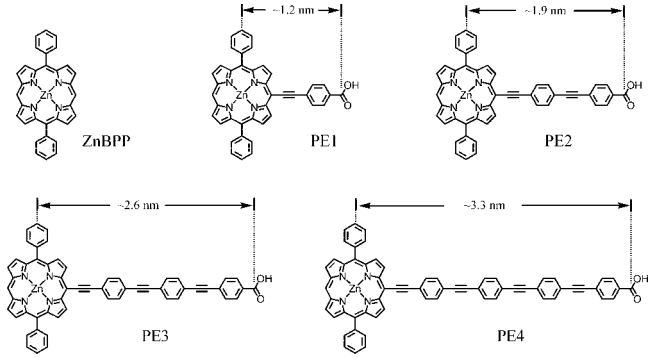

2. Results and Discussion

2.1. Synthesis. To prepare PE1−PE4, we reacted porphyrin precursors with carboxyphenylethynyl reagents according to the Sonogashira cross-coupling method.[13] This synthetic strategy, which is well developed for preparing porphyrins with varied ethyne-linked functional groups,[14,15] was readily adaptable to the synthesis of PE1−PE4. Among a few points worth noting, cross-coupling ZnBPPBr with a suitable substituent precursor effectively yielded PE1 and PE2, but reacting 5-(4-ethynyl-phenylethynyl)-ZnBPP with 4-(4-iodo-phenylethynyl)-benzoic acid seemed to be the most efficient approach to prepare PE3. Our attempts to synthesize PE3 by other routes were unsuccessful because of small yields and the difficulty of recognizing and separating the reaction products. For PE4, the strategy was simply to add a further phenyl group to the porphyrin precursor from the PE3 synthesis. Because of the carboxylic group, these porphyrins all tend to adsorb slightly on the silica gel used in chromatographic purification; the number of chromatographic separations should thus be kept to a minimum to ensure acceptable yields of the porphyrins.

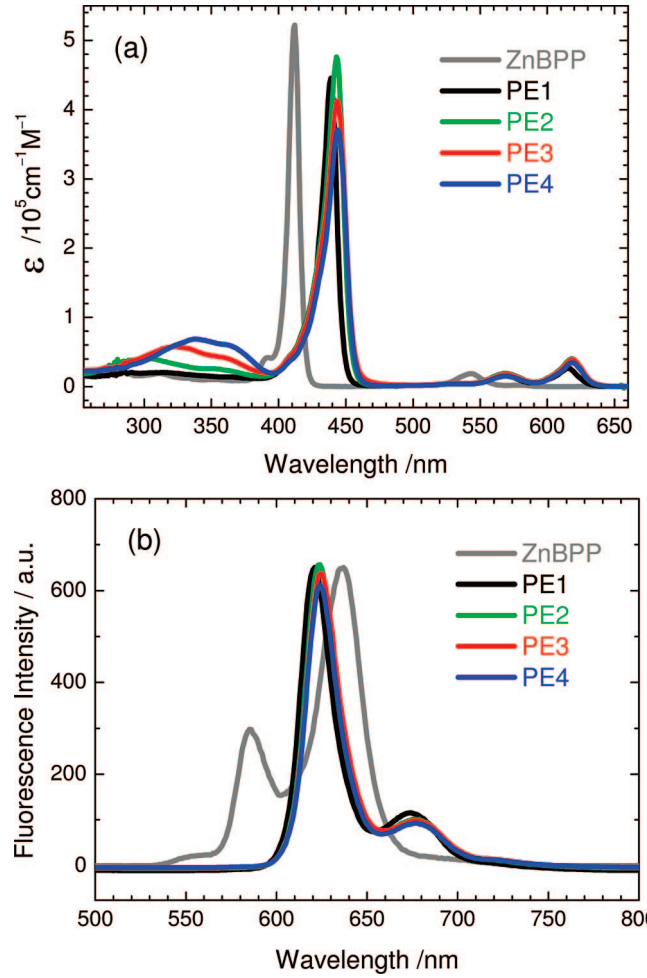

Figure 1. (a) UV−visible absorption and (b) fluorescence spectra of ZnBPP (gray), PE1 (black), PE2 (green), PE3 (red), and PE4 (blue) in THF with $\lambda_{ex} = 430$ nm.

2.2. Absorption and Emission Spectra of Porphyrins in Solution. Parts a and b of Figure 1 show absorption and emission spectra of ZnBPP and PE1−PE4 in tetrahydrofuran (THF), respectively. The absorption maxima and absorption coefficients of these porphyrins are listed in Table 1; the emission maxima and lifetimes of excited states are listed in Table 2. As shown in the figures, these molecules exhibit characteristic porphyrin spectra:[16] strong Soret (B) bands near 440 nm and weaker Q bands in the region of 550−650 nm. The fluorescence spectra show mirror images of the Q bands. Absorption bands of PE1−PE4 are red-shifted from those of

TABLE 1: Absorption Maxima and Absorption Coefficients[a] of Zinc Porphyrins in THF

dye	near-UV bands	λ_{S2} (log ϵ)/nm	λ_{S1} (log ϵ)/nm
ZnBPP	not observed	412 (5.71)	543 (4.27), 579 (3.34)
PE1	not observed	439 (5.64)	567 (4.21), 616 (4.41)
PE2	304, 353	443 (5.67)	569 (4.27), 618 (4.60)
PE3	322, 359	443 (5.58)	569 (4.21), 619 (4.56)
PE4	338, 363	444 (5.56)	569 (4.17), 619 (4.53)

[a] The absorption coefficient (ϵ) has a unit of cm^{-1} M^{-1}.

TABLE 2: Fluorescence Maxima and Lifetimes[a] of the Excited State of Zinc Porphyrins in THF

dye	emission /nm	τ_{S2}/ps	τ_{S1}/ns
ZnBPP	636, 699		
PE1	621, 674	0.91	1.90
PE2	624, 678	0.68	2.10
PE3	624, 677	0.61	2.10
PE4	624, 677	0.60	2.10

[a] S_2 and S_1 lifetimes were monitored at 460 and 620 nm, respectively.

ZnBPP; this shift is due to the extended π-conjugation, consistent with reports of other ethyne-linked porphyrins.[15] Most importantly, the features in the absorption and emission spectra of PE1−PE4 have similar shapes and intensities, indicating that the energy gaps between the ground and the excited states of those porphyrins are similar despite the varied lengths of the PE links.

Further weak absorptions appear in the near-UV region for PE1−PE4; their wavelengths increased systematically as the conjugation length of the PE bridge increased from PE1 to PE4. From PE2 to PE4 the intensities of these near UV absorptions increased, whereas the intensities of the Soret bands decreased, indicating the existence of strong coupling between the PE bridge and the porphyrin core, so that the intensity of the former becomes "borrowed" from the intensity of the latter. As there is no such absorption in ZnBPP, we infer that these near UV absorptions arise from the PE groups of the PE1−PE4 porphyrins. Nielsen et al. reported a similar phenomenon for a zinc porphyrin linked with poly(phenylenethynylene).[17] In the case of PE1−PE4, the coupling and interaction between the bridging moiety and the porphyrin core are effective because similar emission spectra, as shown in Figure 1b, were obtained when those porphyrins were excited in the near -UV region at 350 nm.

2.3. Relaxation Dynamics of Porphyrins in Solutions. Parts a−d of Figure 2 show fluorescence transients of PE1−PE4 in THF, respectively. Those transients were recorded with excitation in the Soret band at λ_{ex} = 420 or 430 nm and emission observed at either λ_{em} = 460 or 620 nm. The transients observed at λ_{em} = 460 nm (circles) are satisfactorily fitted with a single exponential decay convoluted with the instrument-response function (fwhm = 220 fs), which yields decay coefficients 910, 680, 610, and 600 fs for PE1−PE4, respectively. The transients observed at λ_{em} = 620 nm (squares) differ remarkably from the transients observed at λ_{em} = 460 nm (circles): the former show a rising feature with a rise coefficient comparable to the decay coefficient of the latter at short times, but the transient signals of the former increase gradually to an asymptotic level at longer times in the same range. According to femtosecond investigations reported elsewhere,[8a] the transients observed at λ_{em} = 460 and 620 nm reflect the dynamical behavior occurring in electronic states S_2 and S_1 of PE1, respectively. We thus conclude that internal conversion (IC) $S_2 \rightarrow S_1$ of PE1−PE4 in

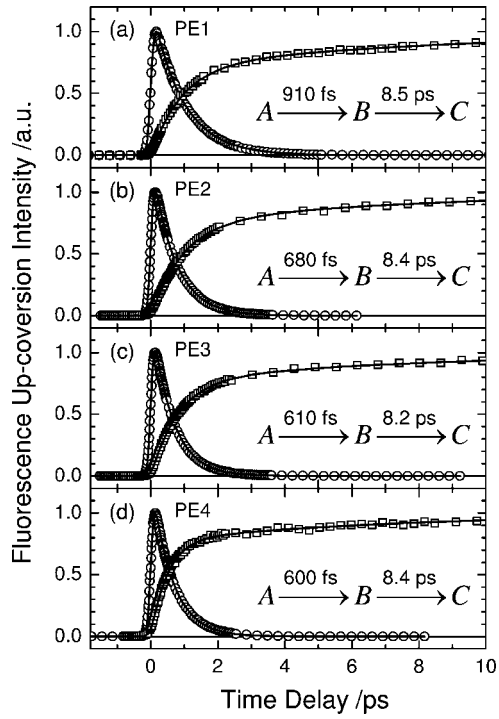

Figure 2. Femtosecond fluorescence transients of (a) PE1, (b) PE2, (c) PE3, and (d) PE4 in THF solution ($c = 1 \times 10^{-5}$ M). Open symbols denote raw data: circles, points obtained at λ_{ex} = 420 nm and λ_{em} = 460 nm; squares, points obtained at λ_{ex} = 430 nm and λ_{em} = 620 nm. The solid curves represent theoretical fits with convolution of the laser pulse.

solution occurs within the observed interval τ = 0.6−0.9 ps and that vibrationally hot S_1 species are produced on that time scale. τ decreased significantly from PE1, τ = 910 fs, to PE2, τ = 680 fs, but only slightly further to ~600 fs for PE3 and PE4. This dynamical feature is consistent with the trend of the spectral shift of the absorption and emission spectra shown in Figure 1b in which the spectra are almost identical for PE2−PE4, but the spectrum of PE1 is somewhat blue-shifted with respect to the others. The systematic decrease of S_2 relaxation periods with increasing length of the PE bridge of PE1−PE4 implies that the electronic coupling of the extended π-conjugation significantly affects the IC rate for $S_2 \rightarrow S_1$, i.e., a longer bridge produces stronger coupling between the porphyrin core and the PE link that leads to a greater rate of internal conversion.

Because of the rising character of the transients shown in Figure 2, the transients observed at λ_{em} = 620 nm are described satisfactorily according to a consecutive kinetic model, $A \rightarrow B \rightarrow C$, with the signals convoluted with the laser pulse. For PE1, the first component (B) rises with τ_1 = 910 fs and decays with τ_2 = 8.5 ps, whereas the second component (C) appears following the decay of the first component but persists on a scale with $\tau_3 \approx$ 2 ns (Table 2); for PE2−PE4, τ_1 = 680, 610, and 600 fs and τ_2 = 8.4, 8.2, and 8.4 ps, respectively. As the fluorescence transients observed at λ_{em} = 620 nm reflect the relaxation dynamics of PE1−PE4 in the S_1 state, the observed two consecutive components (B and C) might be assigned to hot and cold S_1 species, respectively; component A represents the S_2 species not observed at λ_{em} = 620 nm. Accordingly, the hot S_1 species were produced from the S_2 state in 910−600 fs. The excess vibrational energies in the hot S_1 species become released to the solvent molecules via vibrational relaxation, and this process yields the cold S_1 species produced in ~8.5 ps.

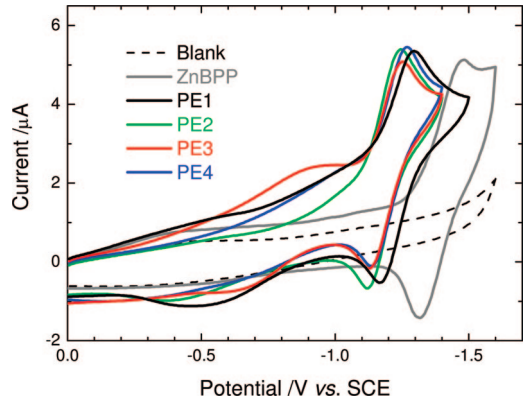

Figure 3. Cyclic voltammograms of ZnBPP and PE1−PE4 reductions in THF.

TABLE 3: First Electrochemical Potentials/V of Zinc Porphyrins in THF[a]

dye	$E_{1/2}$(ox 1)	$E_{1/2}$(red 2)
ZnBPP	0.99 (170 mV)	−1.40 (160 mV)
PE1	∼1.07 (E_{pa})	−1.23 (130 mV)
PE2	∼1.07 (E_{pa})	−1.18 (125 mV)
PE3	∼1.07 (E_{pa})	−1.19 (130 mV)
PE4	∼1.07 (E_{pa})	−1.20 (130 mV)

[a] Experimental conditions: zinc porphyrin (0.5 mM) in freshly distilled and degassed THF/TBAP, scan rate = 100 mV/s, Pt working and counter electrodes, SCE reference electrode. For ferrocene/forrocenium (Fc/Fc^+) in the same conditions, $E_{1/2}$ = +0.49 V vs SCE. Peak-to-peak separations (mV) are shown in parentheses for quasireversible reactions. For irreversible reactions, only the anodic peak potentials, denoted E_{pa}, are shown.

The cold S_1 species endure because $S_1 \rightarrow T_1$ intersystem crossing of PE1−PE4 in solution occurs in ∼2 ns, as confirmed by our picosecond measurements. Our direct observation on the PE1−PE4 system is consistent with femtosecond results for the ZnTPP system, for which the lifetime of the S_2 state of ZnTPP was reported in a range 1.45−2.35 ps, and vibrational cooling from the nonrelaxed vibronic state of the hot S_1 species occurs on a time scale ∼10 ps.[18−20]

2.4. Electrochemistry, DFT Calculations, and Energy Levels. Figure 3 displays cyclic voltammograms (CV) for PE1−PE4 reductions in THF, and Table 3 presents their electrochemical potentials. The first reduction of ZnBPP gave a quasireversible couple at −1.40 V vs SCE, consistent with the formation of the tetraphenylporphinato zinc(II) anion radical at −1.31 V.[21] For PE1−PE4, reduction of the first porphyrin ring occurs at about −1.20 V.[22] The positive shift of the reduction potentials is attributed to the extended π-conjugation. In contrast, the first oxidations of PE1−PE4 are all irreversible reactions (not shown), likely due to THF being capable of attacking the oxidized products. Nevertheless, the oxidation potentials of all these complexes are similar: E_{pa} = +1.07 V vs SCE, Table 3.

To assist our qualitative understanding of the reduction behaviors of these complexes, we performed calculations with DFT on ZnBPP and PE1−PE4 at the B3LYP/LanL2DZ level. Figure 4 depicts their MO patterns from HOMO-1 to LUMO+2. These MO patterns of PE1−PE4 are consistent with those predicted by Gouterman's four-orbital model,[16] i.e., HOMO-1 and HOMO resemble those of the a_{1u} and a_{2u} orbitals, respectively, whereas LUMO and LUMO+1 are similar to those of the e_g orbitals. The HOMO and LUMO of PE1−PE4 are, however, partially delocalized from the porphyrin core to the substituents; this minor deviation from Gouterman's four-orbital model is rationalized through the decreased symmetry of the complexes and the extended π-conjugation of the substituents. LUMO+2 was found to be concentrated at the π-conjugated substituents, consistent with the result of Wang et al. based on a time-dependent DFT approach for a series of β-substituted zinc porphyrins.[4c]

Figure 5 compares the energy levels of PE1−PE4 and TiO_2. This illustration was prepared on the basis of the electrochemical results and the absorption spectra according to literature methods.[23,24] Figure 5 shows that the conducting band (CB) of TiO_2 is located between the LUMO and the HOMO of PE1−PE4, and the MO energy levels between PE1−PE4 are similar, consistent with the DFT results. These results indicate that electron injection from LUMO of the porphyrin to the CB of TiO_2 is feasible and that the rate of electron injection for such a process might be similar for PE1−PE4/TiO_2 films because of their similar energy levels.

2.5. Absorption Spectra of Porphyrins on TiO_2 Nanocrystalline Films. Figure 6 displays UV−visible absorption spectra of PE1−PE4/TiO_2 nanocrystalline films in air (black curves) and PE1−PE4 in THF (gray curves). Comparison of the film spectra with the solution spectra reveals that the Q bands of the PE1−PE4/TiO_2 films are only slightly shifted and broadened from those of the solution spectra, whereas the B bands became blue-shifted with a red shoulder. These shoulders of the Soret bands in the film spectra represent a small proportion of monomeric porphyrins adsorbed on TiO_2 films; their wavelengths are the same as those of the B bands in solution.[25] In spectra of PE1−PE4 films the blue-shifted B bands occur at 413, 415, 420, and 426 nm, respectively. These bands are not caused by effects of reflection[26] because the quality of TiO_2 films (e.g., thickness) seems to have only a slight effect on the intensities. We suggested previously an attribution of these blue-shifted B bands to the H-aggregation of the porphyrin assembly on the surfaces of TiO_2 nanocrystalline films.[8b] The stacked, face-to-face porphyrin π-aggregation (H-type) is well documented to produce a blue shift of the absorption, whereas the side-by-side porphyrin π-aggregation (J-type) results in a red shift.[27] This phenomenon has been observed for not only porphyrins[28] but also other planar dyes.[29] Measurements[8b] with atomic-force microscopy show little variation of morphology between bare TiO_2 nanocrystalline film surfaces and those modified with porphyrin, indicating that the film surfaces are covered with a porphyrin monolayer (thickness only 1−3 nm), supporting the possibility of porphyrins being H-aggregated on the surfaces.

2.6. Relaxation Dynamics of Porphyrins on TiO_2 Nanocrystalline Films. To investigate the dependence of the relaxation dynamics of porphyrin/TiO_2 films on the length of the PE link, we sensitized the four porphyrins on identical TiO_2 nanocrystalline films. Figure 7 shows a scanning electron microscopy image of a typical TiO_2 film (thickness ∼5 μm) with nanoparticle size ∼20 nm. Figure 8 shows the absorption spectra of the four porphyrin-sensitized films with the absorbance of the Q(0,0) band adjusted to be equal for PE1−PE4. Parts a−d of Figure 9 show the fluorescence transients of PE1−PE4 on TiO_2 nanoscrystalline films, respectively, obtained with excitation at λ_{ex} = 420 nm and emission observed at λ_{em} = 470 nm. The transients observed at λ_{em} = 470 nm (circles) are satisfactorily fitted with a single exponential decay convoluted with the instrument response function (fwhm = 220 fs), which yields decay coefficients smaller than 100 fs for all porphyrins. According to our previous work,[8a] the S_2 dynamics of the PE1/

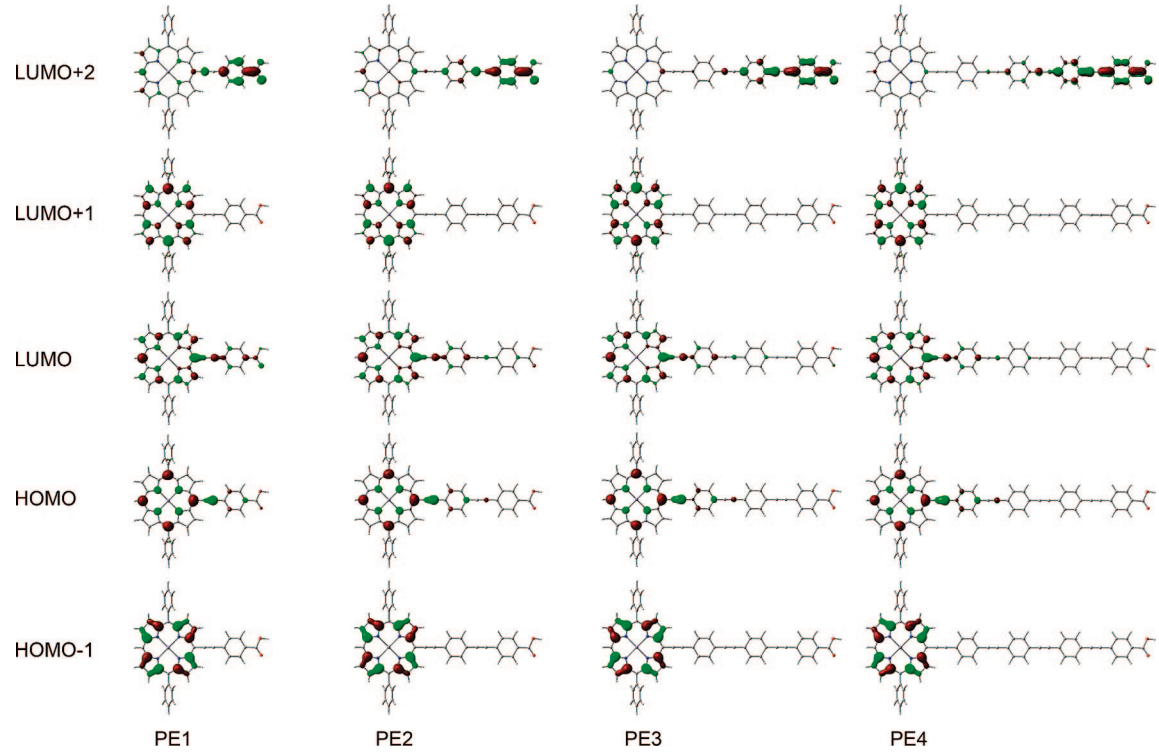

Figure 4. Molecular orbitals of PE1−PE4 with geometries of each molecule optimized at the B3LYP/LanL2DZ level of theory.

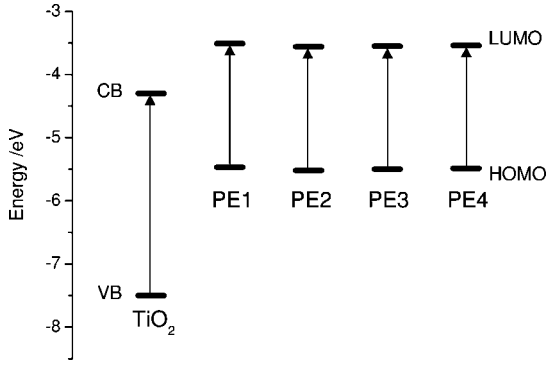

Figure 5. Energy-level diagram of PE1−PE4 showing the HOMO and the LUMO of each porphyrin and the valence band (VB) and conducting band (CB) of TiO_2.

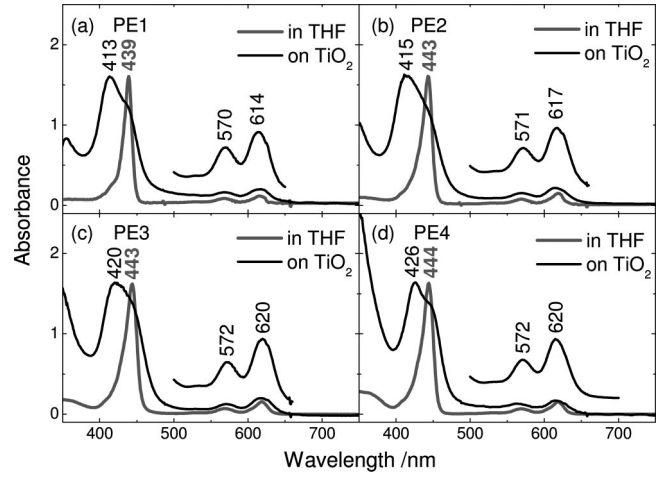

Figure 6. Comparison of absorption spectra of PE1−PE4 on TiO_2 nanocrystalline films (black) and in THF (gray) for (a) PE1, (b) PE2, (c) PE3, and (d) PE4.

TiO_2 films reflect not only the aggregate-induced energy transfer among pophyrins but also an interfacial electron transfer from porphyrin to TiO_2. Because the fluorescence transients were observed also at the S_1 state (see below), we conclude that the $S_2 \rightarrow S_1$ IC is ultrarapid, <100 fs. In the present work we extended the investigation of the S_2 dynamics to porphyrins with an extended PE bridge. The length of the PE group did not affect the observed S_2 dynamics, which are due mainly to the ultrarapid aggregate-induced IC relaxation for all our porphyrin/TiO_2 films. The hot S_1 species were thus produced in <100 fs, and the relaxation dynamics occurring at the porphyrin/TiO_2 interface were probed as described in the following.

Figures 10 and 11 show the S_1 relaxation dynamics of porphyrin/TiO_2 films probed at λ_{em} = 620 and 680 nm, respectively, with PE1−PE4 for parts a−d in each figure (λ_{ex} = 430 nm). All fluorescence transients were fitted with two decay components and a tiny offset. At λ_{em} = 620 nm, the rapid-decay coefficient τ_1 was observed to be 180 fs for PE1, remaining almost constant from PE2 (τ_1 = 200 fs), PE3 (τ_1 = 190 fs), and PE4 (τ_1 = 170 fs); the slow-decay coefficient τ_2 increased slightly from 1.2 ps for PE1 to 1.6 ps for PE4, but the variation was within experimental error. At λ_{em} = 680 nm, τ_1 was in a range 390−540 fs for PE1−PE4 and τ_2 in a range 2.7−3.7 ps for PE1−PE4. The relaxation dynamics observed at 620 nm are much more rapid than those observed at 680 nm because the detection window at the former wavelength probed more "hot" species than that at the latter wavelength.[30]

Two contributions are responsible for the observed S_1 dynamics: interfacial electron transfer from dye to TiO_2 (electron injection) and aggregate-induced energy transfer among dye molecules.[8a] Because the TiO_2 films were prepared identically and the absorbances of the dye were similar for PE1−PE4 (Figure 8), we expect that the amounts of dye loading on TiO_2 films were also similar for PE1−PE4. By assumption that the extents of aggregation inside the nanoporous environment of the TiO_2 films were similar for PE1−PE4, our observations thus indicate that electron injection occurring in the S_1 state might be independent of the length of the link between porphyrin and

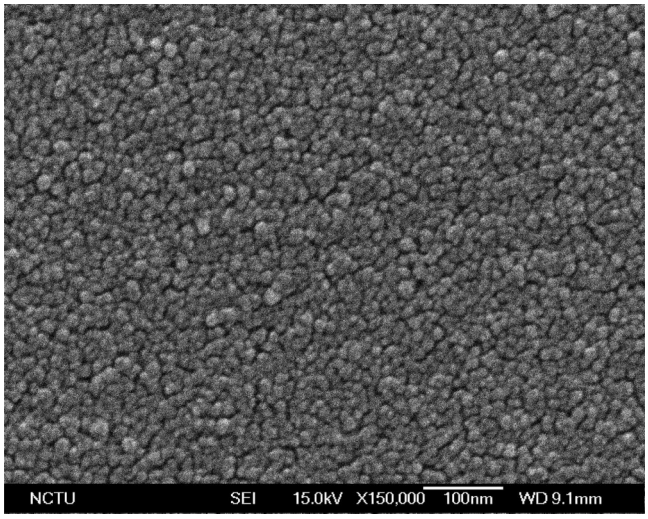

Figure 7. SEM image of TiO_2 nanoparticles spin-coated on a glass plate showing the average particle size ~20 nm. The films (10 layers with thickness ~5 μm) were prepared using the same procedure for sensitization of the dye molecules (PE1−PE4) on the films with equal quality from film to film for fs fluorescence measurements.

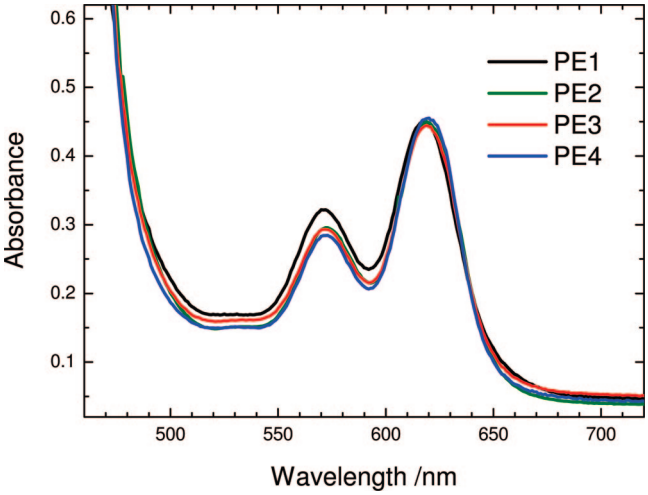

Figure 8. Visible absorption spectra of TiO_2 nanocrystalline films sensitized with PE1−PE4 as indicated.

TiO_2. DFT calculations (Figure 4) indicate, however, that the electron densities of the HOMO and LUMO are localized in the porphyrin ring and extend only to the first unit of the PE link. The detection window of the time-resolved emission occurring from the S_1 state was therefore limited mainly to the porphyrin core. When the electron transfer occurred from the porphyrin moiety to the anchoring group through the PE link, the emission decay might reflect only the initial propagation of electrons in the excited state and thus lack sensitivity for the detection of electron transfer toward longer links.

From the measurement of transient absorption, Galoppini and co-workers[11e] found that the biexponential decays of a Ru-bpy/TiO_2 system occur on a scale of 10−100 ps, and the time coefficients decreased with increasing length of the rigid π-conjugated PE links. The discrepancy between our results (porphyrin/PE/TiO_2) and their results (Ru-bpy/PE/TiO_2) might be due to the detection window, which is much broader using a transient absorption method than using an emission decay method. As a result, the length-dependent trend of electron transfer through PE links of varied length was observed from the former method reported by Galoppini.[11e] Alternatively, if

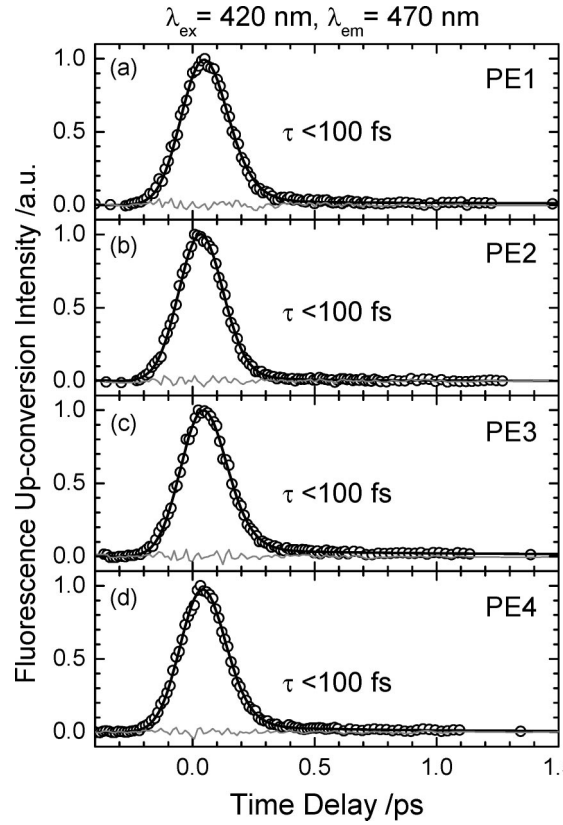

Figure 9. Femtosecond fluorescence transients of (a) PE1, (b) PE2, (c) PE3, and (d) PE4 on TiO_2 nanocrystalline films. Open circles denote raw data obtained at $\lambda_{ex} = 420$ nm and $\lambda_{em} = 470$ nm. The solid curves represent theoretical fits with convolution of the laser pulse.

the electron transfer though the PE link is not a kinetic bottleneck, the discrepancy might reflect the varied number of anchoring groups in the dyes and the structure of the links on the TiO_2 surface, which might affect also the electron injection kinetics. For perylene/TiO_2 films Gundlach et al.[31] found that the rate of electron injection of a rigid-rod system is much greater than that of a tripod system, providing evidence for the variation of electron injection kinetics with structure of the anchoring groups. The dependence of the performance of the porphyrin-sensitized solar cells on the length of the link is discussed in the following section.

2.7. Photovoltaic Performance of Porphyrin-Sensitized Solar Cells. By use of PE1−PE4 as sensitizers, we fabricated DSSC devices according to a standard procedure described in the experimental section. To demonstrate the reproducibility of the data, three independent measurements were performed for each dye using TiO_2 films fabricated with an identical procedure. The measured photovoltaic performances of the DSSC devices with PE1−PE4 are shown in parts a−d of Figure 12; the corresponding parameters are summarized in Table 4. As a reference, the average value of η of the Zn-3-sensitized DSSC was 4.0 ± 0.2%, which is smaller than the literature value (η = 5.2%)[4c] because of thinner TiO_2 films without addition of the scattering layer in our case. The efficiencies of power conversion of the devices decreased greatly, from 2.5 ± 0.2 (PE1), 2.0 ± 0.1 (PE2), 0.78 ± 0.09 (PE3), to 0.25 ± 0.02% (PE4). This systematic variation of the cell performance reflects the photocurrent density, which decreased from 6.6 ± 0.6 (PE1), 5.5 ± 0.1 (PE2), 2.0 ± 0.3 (PE3), to 0.70 ± 0.03 mA cm^{-2} (PE4) as the length of the PE link increased from d /nm = 1.2 (PE1), 1.9 (PE2), 2.6 (PE3), to 3.3 (PE4). Our results unambiguously demonstrate that the cell performance depends directly

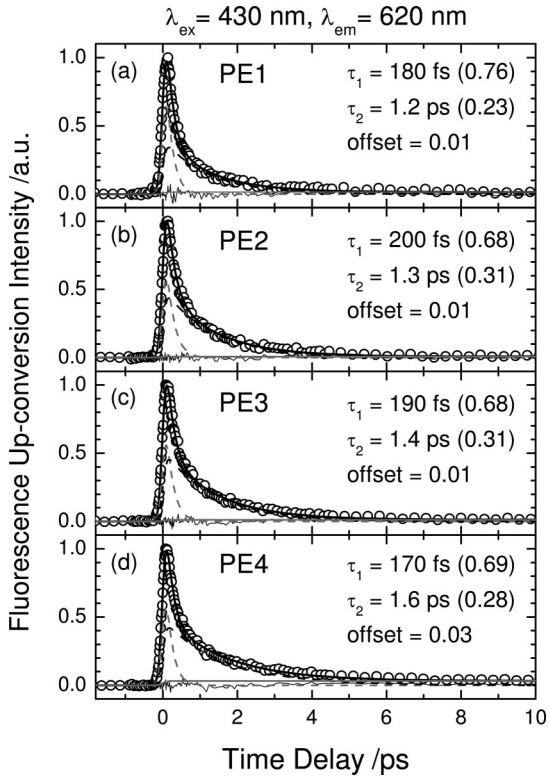

Figure 10. Femtosecond fluorescence transients of (a) PE1, (b) PE2, (c) PE3, and (d) PE4 on TiO_2 nanocrystalline films. Open circles denote raw data obtained at $\lambda_{ex} = 430$ nm and $\lambda_{em} = 620$ nm. The solid and dashed curves represent theoretical fits with convolution of the laser pulse.

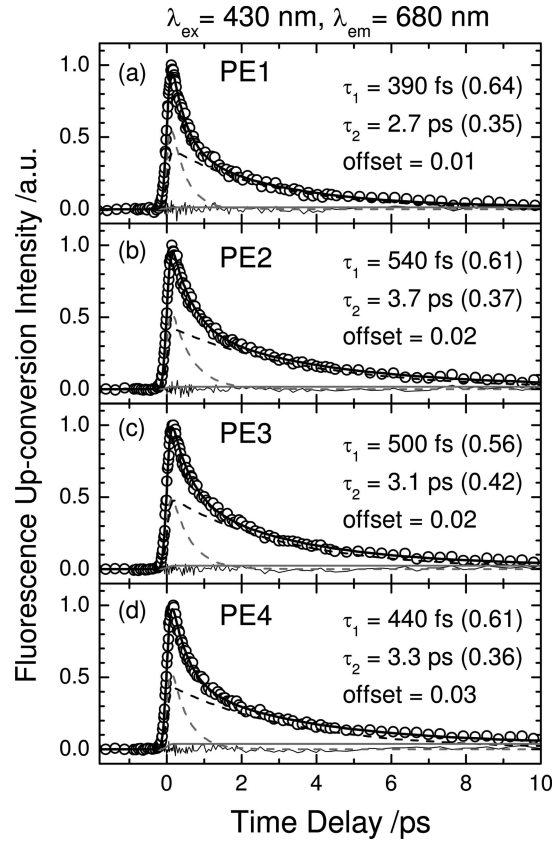

Figure 11. Femtosecond fluorescence transients of (a) PE1, (b) PE2, (c) PE3, and (d) PE4 on TiO_2 nanocrystalline films. Open circles denote raw data obtained at $\lambda_{ex} = 430$ nm and $\lambda_{em} = 680$ nm. The solid and dashed curves represent theoretical fits with convolution of the laser pulse.

on the length of a rigid π-conjugated link: the longer the link, the poorer the cell performance becomes. The observed length-dependent photovoltaic performance of the porphyrin-based DSSC is similar to the trend reported for a rigid planar meta-substituted porphyrin/TiO_2 system,[11f] for which a short link with enhanced photovoltaic efficiency was attributed to increased efficiency of electron injection from porphyrin to TiO_2.

We measured the conversion efficiency of incident photons to current (IPCE) for the devices with PE1 and PE4 in the wavelength range 400−800 nm; the results appear in Figure 13. The photocurrent action spectra of the PE1 and PE4 devices mimic their corresponding absorption spectra, but the IPCE values of PE1 are ten times those of PE4, consistent with the difference in J_{SC} and η for these two devices. The IPCE is expressible in terms of the light-harvesting efficiency (LHE), the quantum yield of electron injection (ϕ_{inj}), and the efficiency of charge collection at the counter electrode (η_c) according to[2]

$$\mathrm{IPCE}(\lambda) = \mathrm{LHE}(\lambda)\varphi_{inj}\eta_c \quad (1)$$

As the absorbances of all sensitized films are similar, the values of LHE of all porphyrin-sensitized films are similar. If the rates of electron injection are similar for PE1−PE4, the ϕ_{inj} values for all porphyrin-sensitized films are likewise similar. The factor affecting the IPCE values and other photovoltaic parameters (J_{SC} and η) between PE1 and PE4 might be due to η_c, which is dependent upon both the rate of charge recombination from the reduced TiO_2 nanoparticles to the oxidized porphyrin and the rate of dye regeneration by the oxidation of electrolyte.[11f] For the dependence on distance of the open-circuit voltage in a tripodal sensitizer system, Clark et al. found that V_{OC} was much greater for a device with a longer PE link.[32] In general, V_{OC} is larger if the dye regeneration ($dye^+ + e^- \rightarrow$ dye) due to oxidation ($3I^- \rightarrow I_3^- + 2e^-$) occurs over a greater distance from the TiO_2 surface. The charge recombination between $TiO_2(e^-)$ and I_3^- would hence be much slower over a greater distance so as to increase the efficiency of dye regeneration for the sensitizer with a longer link. We found, however, that V_{OC} in porphyrin-sensitized SC was even smaller in the porphyrin with the longest link (PE4), in contrast with the results reported for the Ru-bpy/TiO_2 system.[32] The smaller J_{SC} observed for the device with a longer PE link might reflect much more

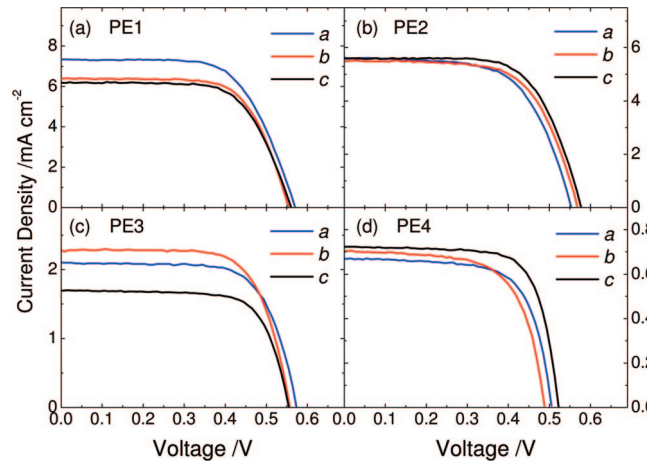

Figure 12. *IV* curves of porphyrin-sensitized SC for (a) PE1, (b) PE2, (c) PE3, and (d) PE4. Three independent measurements were conducted with the same TiO_2 films (labeled a−c, Table 4); devices were fabricated with the same procedure. All data were collected under one solar AM1.5 illumination (100 mW cm^{-2}) with active area 0.25 cm^2.

TABLE 4: Photovoltaic Parameters of Porphyrin-Based DSSCs under AM1.5 Illumination (Power 100 mW cm^{-2}) and Active Area 0.25 cm^2

dye	films	J_{SC}/mA cm^{-2}	V_{OC}/V	FF	η/%
Zn3	a	9.4	0.65	0.62	3.78
	b	10.5	0.63	0.63	4.17
	c	10.1	0.65	0.62	4.07
	average	10.0 ± 0.6	0.64 ± 0.01	0.62 ± 0.01	4.0 ± 0.2
PE1	a	7.3	0.57	0.65	2.70
	b	6.4	0.55	0.68	2.39
	c	6.2	0.56	0.67	2.33
	average	6.6 ± 0.7	0.56 ± 0.01	0.67 ± 0.02	2.5 ± 0.2
PE2	a	5.6	0.58	0.66	2.14
	b	5.5	0.57	0.65	2.04
	c	5.6	0.55	0.62	1.91
	average	5.5 ± 0.1	0.57 ± 0.02	0.64 ± 0.02	2.0 ± 0.1
PE3	a	2.1	0.57	0.70	0.84
	b	2.3	0.56	0.70	0.82
	c	1.7	0.56	0.72	0.68
	average	2.0 ± 0.3	0.56 ± 0.01	0.70 ± 0.01	0.78 ± 0.09
PE4	a	0.67	0.51	0.69	0.24
	b	0.70	0.49	0.66	0.23
	c	0.72	0.52	0.73	0.27
	average	0.70 ± 0.03	0.51 ± 0.02	0.69 ± 0.04	0.25 ± 0.02

rapid electron transfer from TiO_2 back to the dye cation. The kinetics of charge recombination for the system reported here are thus of great interest; this work is in progress.

3. Conclusion

Novel porphyrins (PE1−PE4) were designed and synthesized for the purposes of investigating the interfacial electron-transfer and DSSC applications. The porphyrins involve a ZnBPP moiety as a light-harvesting center and a carboxylic acid as an anchoring group with the π-conjugated PE units serving as a link to control the distance between the porphyrin core and the TiO_2 surface. When these porphyrins were fabricated into DSSC devices, the efficiencies of power conversion of these devices decreased systematically from 2.5 ± 0.2% for PE1 to 0.25 ± 0.02% for PE4. Measurements of femtosecond fluorescence of the porphyrin-sensitized TiO_2 films showed that the emission decays of the system are similar for PE1−PE4, indicating that electron injection from the porphyrin core to the surface of TiO_2 might be equally rapid for PE1−PE4. DFT calculations indicate that electron densities are localized on the porphyrin core and the first PE link, which might indicate that our observations reflect a narrow detection window that lacks sensitivity to probe electron transfer through links of varied length. Although a slow electron injection in a long link might occur at the dye/TiO_2 interface, as Galoppini and co-workers[11e] and Gundlach et al.[31] reported, other factors must be considered to account for the great degradation of performance in the devices with a long PE link.

4. Experiments

4.1. Materials. Solvents CH_2Cl_2, $CHCl_3$, and ethyl acetate (ACS grade, Mallinckrodt Baker, Kentucky, USA), hexanes (Haltermann, Hamburg, Germany), and THF (Merck, Darmstadt, Germany) in the syntheses were used as received unless otherwise stated. THF and tetrabutylammonium perchlorate (TBAP) were purified according to literature methods.[33] Pd(PPh_3)$_4$ catalyst (Strem Chemical Inc., MA, USA), silica gel 60 for chromatographic purification (230−400 mesh, Merck), and other chemicals (Acros Organics, NJ, USA) were obtained from the indicated suppliers.

4.2. General Syntheses. The Sonogashira cross-coupling method was used to perform most reactions:[13] 5-bromo-10,20-biphenylporphinato zinc(II) (ZnBPPBr, 100 mg) under dinitrogen was typically mixed with ethynyl substituents (2−4 equiv), Pd(PPh_3)$_4$ (20 mol%), CuI (10 mol%), and Et_2NH (5 mL) in freshly distilled THF (75−85 mL). The degassed reaction mixtures were stirred under dinitrogen at 40 °C and monitored with thin-layer chromatography and UV−visible spectra. Upon completion, the reactions were quenched with $NH_4Cl_{(aq)}$ washes followed by chromatographic separation on silica gel with CH_3OH/CH_2Cl_2 eluents and crystallization from THF/hexanes.

PE1 was synthesized on cross-coupling ZnBPPBr and 4-ethynylbenzoic acid in 80% yield. 4-Ethynylbenzoic acid was obtained from cross-coupling trimethylsilylacetylene with 4-iodobenzoic acid (78%) with deprotection from tetrabutylammonium fluoride (TBAF/ THF) in 82% yield. ^{1}H NMR (d_6-DMSO at 2.50 ppm) δ/ppm 10.36 (s, 1H), 9.84 (d, J 5 Hz, 2H), 9.46 (d, J 5 Hz, 2H), 8.92 (d, J 5 Hz, 2H), 8.84 (d, J 5 Hz, 2H), 8.25 (m, 8H), 7.86 (m, 6H). Anal. $C_{41}H_{24}N_4O_2Zn \cdot C_4H_8O$: calcd. C 72.83%, H 4.35%, N 7.55%; found C 72.35%, H 4.60%, N 7.27%. Visible absorption/nm: 439 (log ϵ/cm^{-1} M^{-1} = 5.64), 567 (4.21), 616 (4.41).

PE2 was prepared from ZnBPPBr and 4-(4-ethynyl-phenylethynyl)benzoic acid in 32% yield. 4-(4-Ethynyl-phenylethynyl)benzoic acid was generated on cross-coupling 4-ethynylbenzoic acid with 1,4-diethynylbenzene (65%). Cross-coupling 1,4-diiodobenzene with trimethylsilylacetylene yielded 1,4-bis(trimethylsilylethynyl)benzene in nearly 100% yield. The deprotection reaction in TBAF/THF gave 1,4-diethynylbenzene (81%) after chromatographic separation. ^{1}H NMR (d_6-DMSO at 2.50 ppm) δ/ppm 10.34 (s, 1H), 9.38 (d, J 5 Hz, 2H), 9.45 (d, J 5 Hz, 2H), 8.90 (d, J 5 Hz, 2H), 8.83 (d, J 5 Hz, 2H), 8.20 (t, J 4 Hz, 6H), 8.01 (d, J 8 Hz, 2H), 7.86 (m, 8H), 7.74 (d, J 8 Hz, 2H). Anal. $C_{49}H_{28}N_4O_2Zn \cdot C_4H_8O$: calcd. C 75.58%, H 4.31%, N 6.65%; found C 75.05%, H 4.27%, N 6.68%. Visible absorption/nm: 443 (log ϵ = 5.67), 569 (4.27), 618 (4.60).

PE3 was obtained on reacting 5-(4-ethynyl-phenylethynyl)-ZnBPP with 4-(4-iodo-phenylethynyl)benzoic acid in 30% yield. 5-(4-Ethynyl-phenylethynyl)-ZnBPP was generated on cross-coupling ZnBPPBr with 1,4-diethynylbenzene at 41% yield. 4-(4-Iodo-phenylethynyl)benzoic acid was produced from 1,4-diiodobenzene and 4-ethynylbenzoic acid in 19% yield. ^{1}H NMR(d_6-DMSO at 2.50 ppm) δ/ppm 10.33 (s, 1H), 9.83 (d, J 5 Hz, 2H), 9.44 (d, J 5 Hz, 2H), 8.90 (d, J 4 Hz, 2H), 8.93 (d,

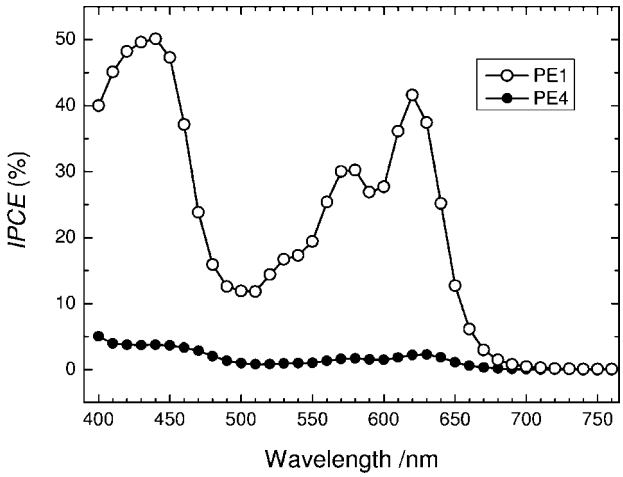

Figure 13. Photocurrent action spectra of PE1- and PE4-sensitized solar cells.

J 4 Hz, 2H), 8.21 (t, *J* 8 Hz, 6H), 7.99 (d, *J* 8 Hz, 2H), 7.85 (overlapped, 8H), 7.69 (overleapped, 6H). Anal: $C_{57}H_{32}N_4O_2Zn \cdot CH_3OH \cdot 3H_2O$: calcd. C 72.82%, H 4.43%, N 5.86%; found C 72.59%, H 4.46%, N 5.26%. Visible absorption/nm: 443 (log ϵ = 5.58), 569 (4.21), 619 (4.56).

PE4 was prepared from 5-[4-(4-iodo-phenylethynyl)-phenylethynyl]-ZnBPP and 4-(4-ethynyl-phenylethynyl)benzoic acid in 38% yield. 5-[4-(4-Iodo-phenylethynyl)-phenylethynyl]-ZnBPP was synthesized on cross-coupling 5-(4-ethynyl-phenylethynyl)-ZnBPP with 1,4-diiodobenzene (yield 39%). 4-(4-Ethynyl-phenylethynyl)benzoic acid was generated on cross-coupling 1,4-diethynylbenzene with 4-iodobenzoic acid (yield 65%). ^{1}H NMR d_6-DMSO at 2.50 ppm δ/ppm 10.34 (s, 1H), 9.83 (d, *J* 4 Hz, 2H), 9.45 (d, *J* 4 Hz, 2H), 8.90 (d, *J* 4 Hz, 2H), 8.82 (d, *J* 4 Hz, 2H), 8.20 (t, *J* 4 Hz, 6H), 7.95 (d, *J* 8 Hz, 2H), 7.86 (overlapped, 8H), 7.66 (overlapped, 10H). Anal. $C_{65}H_{36}N_4O_2Zn \cdot 2H_2O$: calcd. C 77.57%, H 4.01%, N 5.57%; found C 77.61%, H 4.00%, N 5.36%. Visible absorption/nm: 444 (log ϵ = 5.56), 569 (4.17), 619 (4.53).

4.3. Steady-State Spectral Measurements. Absorption spectra (Agilent 8453 UV−visible spectrophotometer), fluoresence spectra (Cary Eclipse fluorescence spectrophotometer), NMR spectra (Varian Unity Inova 300WB NMR spectrometer), and elemental analyses (Elementar Vario EL III) were measured with the indicated instruments. Cyclic voltammograms (CH Instruments Electrochemical Workstation 660A) were recorded with a standard three-electrode cell: a Pt working electrode, a Pt auxiliary electrode isolated from the main compartment by a layer of fine glass frit, and a reference electrode (SCE) isolated from the main compartment by a junction tipped with a platinum wire. A glovebox (M. Braun Unilab), a vacuum line, and standard Schlenk glassware were employed to process all air-sensitive materials.

4.4. Time-Resolved Fluorescence Measurements. Fluorescence decays were recorded with an optically gated (up-conversion) system (FOG100, CDP), described elsewhere.[34] Briefly, the femtosecond laser system (Mira 900D, Coherent) generated output pulses at 860 nm (or 840 nm) of duration ~120 fs at a repetition rate 76 MHz. The frequency of the laser pulse was doubled for excitation (λ_{ex} = 430 or 420 nm). The residual fundamental pulse served as an optical gate; a dichroic beam splitter separated excitation and gate beams. The intensity of the excitation beam was appropriately attenuated and focused onto a rotating cell (optical path of length 1 mm) containing either the solution or the solid thin-film samples. The emission was collected with two parabolic mirrors and focused onto a crystal (BBO type-I); the gate pulse was also focused on that BBO crystal for sum-frequency generation. The latter signal was collected with a lens, separated from interference light with an iris, a band-pass filter, and a double monochromator (DH10, Jobin Yvon) in combination, and then detected with a photomultiplier (R1527P, Hamamatsu) connected to a computer-controlled photon-counting system. By variation of the temporal delay between gate and excitation pulses via a stepping-motor translational stage, we obtained a temporal profile (transient). The polarization between pump and probe pulses was fixed at the magic-angle condition, 54.7°.

4.5. Cell Fabrication and Performance Characterization. Three key components are essential in the construction of a sandwich-type DSSC device: a light-harvesting layer (dye/TiO_2) is deposited on a transparent conducting oxide (TCO) surface to serve as a working electrode (anode); a Pt-coated layer is deposited on a TCO surface to serve as a counter electrode (cathode), and an diiodine-based electrolyte fills the space between the anode and the cathode to serve as a redox couple of the cell. For a working electrode, a TiO_2 nanoparticulate film was produced on a fluoride-doped tin oxide (FTO, 30 Ω/□, Sinonar, Taiwan) glass via screen printing. Crystallization of TiO_2 films (thickness ~6 μm and active area 0.25 cm^2) was performed on annealing in two stages: heating at 450 °C for 5 min followed by heating at 500 °C for 30 min. The TiO_2 film was then immersed in a aqueous solution of $TiCl_4$ (40 mM, 70 °C, 30 min) followed by the same two-stage thermal treatment for final annealing of the electrode. The electrode was then immersed in the dye/THF solution for dye loading onto the TiO_2 film. The Pt counter electrodes were prepared on spin-coating drops of H_2PtCl_6 solution onto FTO glass and heating at 400 °C for 15 min. To prevent a short circuit, the two electrodes were assembled into a cell of sandwich type and sealed with a hot-melt film (SX1170, Solaronix, thickness 25 μm). The electrolyte solution containing LiI (0.1 M), I_2 (0.05 M), BMII (0.6 M), and 4-*tert*-butylpyridine (0.5 M) in a mixture of acetonitrile and valeronitrile (volume ratio 1:1) was introduced into the space between the two electrodes, so completing the fabrication of these DSSC devices.

The performance of a DSSC device was assessed on measurement of an *IV* curve with an AM-1.5 solar simulator (Newport-Oriel 91160). The solar simulator employs filters and other optical components to mimic solar radiation with an air mass 1.5 spectrum; the output intensity is evenly distributed for illumination of a large area. When the device is irradiated with the solar simulator, the source meter (Keithley 2400, computer-controlled) sends a voltage (*V*) to the device, and the photocurrent (*I*) is read at each step controlled by a computer via a GPIB interface. The solar simulator was calibrated with a Si-based reference cell (S1133, Hamamatsu) and an IR-cut filter (KG5) to correct the spectral mismatch of the lamp.[35] The actively illuminated area was 0.25 cm^2 for all measurements.

Acknowledgment. National Science Council of Republic of China (Project Contracts 96-2628-M-009-018-MY2 and 96-2627-M-009-005 for E.W.-G.D. and 95-2113-M-260-006-MY2 and 96-2627-M-260-001 for C.-Y.L.) provided financial support.

References and Notes

(1) O'Regan, B.; Grätzel, M. *Nature* **1991**, *353*, 737.

(2) Nazeeruddin, M. K.; Kay, A.; Rodicio, I.; Humphry-Baker, R.; Muller, E.; Liska, P.; Vlachopoulos, N.; Grätzel, M. *J. Am. Chem. Soc.* **1993**, *115*, 6382.

(3) (a) Wang, Q.; Ito, S.; Grätzel, M.; Fabregat-Santiago, F.; Mora-Seró, I.; Bisquert, J.; Bessho, T.; Imai, H. *J. Phys. Chem. B* **2006**, *110*,

25210. (b) Wei, M.; Konishi, Y.; Zhou, H.; Yanagida, M.; Sugihara, H.; Arakawa, H. *J. Mater. Chem.* **2006**, *16*, 1287. (c) Koide, N.; Islam, A.; Chiba, Y.; Han, L. *J. Photochem. Photobiol. A* **2006**, *182*, 296.

(4) (a) Nazeeruddin, M. K.; Humphry-Baker, R.; Officer, D. L.; Campbell, W. M.; Burrell, A. K.; Grätzel, M. *Langmuir* **2004**, *20*, 6514. (b) Campbell, W. M.; Burrell, A. K.; Officer, D. L.; Jolley, K. W. *Coord. Chem. Rev.* **2004**, *248*, 1363. (c) Wang, Q.; Campbell, W. M.; Bonfantani, E. E.; Jolley, K. W.; Officer, D. L.; Walsh, P. J.; Gordon, K.; Humphry-Baker, R.; Nazeeruddin, M. K.; Grätzel, M. *J. Phys. Chem. B* **2005**, *109*, 15397. (d) Campbell, W. M.; Jolley, K. W.; Wagner, P.; Wagner, K.; Walsh, P. J.; Gordon, K.; Schmidt-Mende, L.; Nazeeruddin, M. K.; Wang, Q.; Pechy, P.; Renouard, T.; Zakeeruddin, S. M.; Grätzel, M.; Officer, D. *J. Phys. Chem. C* **2007**, *111*, 11760.

(5) Odobel, F.; Blart, E.; Lagree, M.; Villieras, M.; Boujtita, H.; Murr, N. E.; Caramori, S.; Bignozzi, C. A. *J. Mater. Chem.* **2003**, *13*, 502.

(6) Bignozzi, C. A.; Argazzi, R.; Kleverlaan, C. J. *Chem. Soc. Rev.* **2000**, *29*, 87.

(7) Cid, J.-J.; Yum, J.-H.; Jang, S.-R.; Nazeeruddin, M. K.; Martínez-Ferrero, E.; Palomares, E.; Ko, J.; Grätzel, M.; Torres, T. *Angew. Chem., Int. Ed.* **2007**, *46*, 8358.

(8) (a) Luo, L.; Lo, C.-F.; Lin, C.-Y.; Chang, I.-J.; Diau, E. W.-G. *J. Phys. Chem. B* **2006**, *110*, 410. (b) Lo, C.-F.; Luo, L.; Diau, E. W.-G.; Chang, I.-J.; Lin, C.-Y. *Chem. Commun.* **2006**, 1430.

(9) (a) Siemsen, P.; Livingston, R. C.; Diederich, F. *Angew. Chem., Int. Ed.* **2000**, *39*, 2632. (b) Bunz, U. H. F. *Chem. Rev.* **2000**, *100*, 1605. (c) Yang, S. I.; Prathapan, S.; Miller, M. A.; Seth, J.; Bocian, D. F.; Lindsey, J. S.; Holten, D. *J. Phys. Chem. B* **2001**, *105*, 8249.

(10) (a) Kim, D.; Osuka, A. *J. Phys. Chem. A* **2003**, *107*, 8791. (b) Holten, D.; Bocian, D. F.; Lindsey, J. S. Acc. Chem. Res. 2002, *35*, 57, and references therein. (c) Loewe, R. S.; Lammi, R. K.; Diers, J. R.; Kirmaier, C.; Bocian, D. F.; Holten, D.; Lindsey, J. S. *J. Mater. Chem.* **2002**, *12*, 1530. (d) Wojaczynski, J.; Latos-Grazynski, L. *Coord. Chem. Rev.* **2000**, *204*, 113. (e) Rubtsov, I. V.; Susumu, K.; Rubtsov, G. I.; Therien, M. J. *J. Am. Chem. Soc.* **2003**, *125*, 2687. (f) Susumu, K.; Therien, M. J. *J. Am. Chem. Soc.* **2002**, *124*, 8550. (g) Screen, T. E. O.; Lawton, K. B.; Wilson, G. S.; Dolney, N.; Ispasoiu, R.; Goodson, T., III.; Martin, S. J.; Bradley, D. D. C.; Anderson, H. L. *J. Mater. Chem.* **2001**, *11*, 312.

(11) (a) Piotrowiak, P.; Galoppini, E.; Wei, Q.; Meyer, G. J.; Wiewior, P. *J. Am. Chem. Soc.* **2003**, *125*, 5278. (b) Hoertz, P. G.; Carlisle, R. A.; Meyer, G. J.; Wang, D.; Piotrowiak, P.; Galoppini, E. *Nano Lett.* **2003**, *3*, 325. (c) Galoppini, E.; Guo, W.; Zhang, W.; Hoertz, P. G.; Qu, P.; Meyer, G. J. *J. Am. Chem. Soc.* **2002**, *124*, 7801. (d) Galoppini, E. *Coord. Chem. Rev.* **2004**, *248*, 1283. (e) Myahkostupov, M.; Piotrowiak, P.; Wang, D.; Galoppini, E. *J. Phys. Chem. C* **2007**, *111*, 2827. (f) Rochford, J.; Chu, D.; Hagfeldt, A.; Galoppini, E. *J. Am. Chem. Soc.* **2007**, *129*, 4655. (g) Rochford, J.; Galoppini, E. *Langmuir* **2008**, *24*, 5366.

(12) Sazanovich, I. V.; Kirmaier, C.; Hindin, E.; Yu, L.; Bocian, D. F.; Lindsey, J. S.; Holten, D. *J. Am. Chem. Soc.* **2004**, *126*, 2664.

(13) (a) Sonogashira, K.; Tohda, Y.; Hagihara, N. *Tet. Lett.* **1975**, 4467. (b) Takahashi, S.; Kuroyama, Y.; Sonogashira, K. *Synthesis* **1980**, 627.

(14) (a) Zhang, T.-G.; Zhao, Y.; Asselberghs, I.; Persoons, A.; Clays, K.; Therien, M. J. *J. Am. Chem. Soc.* **2005**, *127*, 9710. (b) Susumu, K.; Duncan, T. V.; Therien, M. J. *J. Am. Chem. Soc.* **2005**, *127*, 5186. (c) Liu, Z.; Schmidt, I.; Thamyongkit, P.; Loewe, R. S.; Syomin, D.; Diers, J. R.; Zhao, Q.; Misra, V.; Lindsey, J. S.; Bocian, D. F. *Chem. Mater.* **2005**, *17*, 3728. (d) Yasseri, A. A.; Syomin, D.; Malinovskii, V. L.; Loewe, R. S.; Lindsey, J. S.; Zaera, F.; Bocian, D. F. *J. Am. Chem. Soc.* **2004**, *126*, 11944. (e) Screen, T. E. O.; Thorne, J. R. G.; Denning, R. G.; Bucknall, D. G.; Anderson, H. L. *J. Am. Chem. Soc.* **2002**, *124*, 9712. (f) Blake, I. M.; Rees, L. H.; Claridge, T. D. W.; Anderson, H. L. *Angew. Chem., Int. Ed.* **2000**, *39*, 1818. (g) Wilson, G. J.; Arnold, D. P. *J. Phys. Chem. A* **2005**, *109*, 6104. (h) Webb, S. J.; Sanders, J. K. M. *Inorg. Chem.* **2000**, *39*, 5912.

(15) (a) Lin, C.-Y.; Chuang, L.-C.; Lin, Y.-C.; Lin, C.-L. *Dalton Trans.* **2004**, 4006. (b) Lin, C.-Y.; Chuang, L.-C.; Yang, Y.-F.; Lin, C.-L.; Kao, H.-C.; Wang, W.-J. *Dalton Trans.* **2004**, 456. (c) Blake, I. M.; Rees, L. H.; Claridge, T. D. W.; Anderson, H. L. *Angew. Chem., Int. Ed.* **2000**, *39*, 1818. (d) Taylor, P. N.; Wylie, A. P.; Huuskonen, J.; Anderson, H. L. *Angew. Chem., Int. Ed.* **1998**, *37*, 986. (e) LeCours, S. M.; Philips, C. M.; de Paula, J. C.; Therien, M. J. *J. Am. Chem. Soc.* **1997**, *119*, 12578. (f) LeCours, S. M.; Guan, H. W.; DiMagno, S. G.; Wang, C. H.; Therien, M. J. *J. Am. Chem. Soc.* **1996**, *118*, 1497.

(16) Gouterman, M. *J. Mol. Spectrosc.* **1961**, *6*, 138.

(17) Nielsen, K. T.; Spanggaard, H.; Krebs, F. C. *Macromolecules* **2005**, *38*, 1180.

(18) Gurzadyan, G. G.; Tran-Thi, T.-H.; Gustavsson, T. *J. Chem. Phys.* **1998**, *108*, 385.

(19) Mataga, N.; Shibata, Y.; Chosrowjan, H.; Yoshida, N.; Osuka, A. *J. Phys. Chem. B* **2000**, *104*, 4001.

(20) Yu, H.; Baskin, J. S.; Zewail, A. H. *J. Phys. Chem. A* **2002**, *106*, 9845.

(21) (a) Kadish, K. M.; Caemelbecke, E. V.; Royal, G. In *The Porphyrin Handbook*; Kadish, K. M.; Smith, K. M.; Guilard, G., Eds.;Academic Press: New York, 2000; Vol. 8, pp 1−97. (b) Kadish, K. M.; Royal, G.; Caemelbecke, E. V.; Gueletti, L. In *The Porphyrin Handbook*; Kadish, K. M.; Smith, K. M.; Guilard, G., Eds.; Academic Press: New York, 2000; Vol. 9.

(22) We observed ill-defined reduction waves before the porphyrin first ring-reductions; these reduction waves are similar to the reduction waves of the substituents under the same experimental conditions, e.g., 4-iodobenzoic acid, 4-ethynylbenzoic acid, 4-(trimethylsilylethynyl)benzoic acid, and 4-(4-ethynylphenylethynyl)benzoic acid.

(23) (a) Thomas, K. R. J.; Lin, J. T.; Tao, Y.-T.; Ko, C.-W. *J. Am. Chem. Soc.* **2001**, *123*, 9404. (b) Koene, B. E.; Loy, D. E.; Thompson, M. E. *Chem. Mater.* **1998**, *10*, 2235. (c) Thelakkat, M.; Schmidt, H.-W. *Adv. Mater.* **1998**, *10*, 219. (d) Janietz, S.; Bradley, D. D. C.; Grell, M.; Giebeler, C.; Inbasekaran, M.; Woo, E. P. *Appl. Phys. Lett.* **1998**, *73*, 2453.

(24) (a) Hagfeldt, A.; Grätzel, M. *Chem. Rev.* **1995**, *95*, 49. (b) Pommerehne, J.; Vestweber, H.; Guss, W.; Mahrt, R. F.; Bassler, H.; Porsch, M.; Daub, J. *Adv. Mater.* **1995**, *7*, 551.

(25) To avoid saturation of the intensity of the film absorption band, we limited the amount of PE1−PE4 adsorbed onto the TiO_2 plates. Some porphyrins are expected to adsorb on TiO_2 surfaces in monomeric form with a less extent of aggregation.

(26) (a) Donker, H.; Koehorst, R. B. M.; Schaafsma, T. J. *J. Phys. Chem. B* **2005**, *109*, 17031. (b) Donker, H.; Hoek, A.; Schaik, W.; Koehorst, R. B. M.; Yatskou, M. M.; Schaafsma, T. J. *J. Phys. Chem. B* **2005**, *109*, 17038. (c) Schaafsma, T.; Dag, I.; Sitters, R.; Glasbeek, M.; Lifshitz, E. *J. Phys. Chem. B* **2005**, *109*, 17047.

(27) Kasha, M. *Radiat. Res.* **1963**, *20*, 55.

(28) Maiti, N. C.; Mazumdar, S.; Periasamy, N. *J. Phys. Chem. B* **1998**, *102*, 1528.

(29) (a) Chowdhury, A.; Wachsmann-Hogiu, S.; Bangal, P. R.; Raheen, I.; Peteanu, L. A. *J. Phys. Chem. B* **2001**, *105*, 12196. (b) Wang, M.; Silva, G. L.; Armitage, B. A. *J. Am. Chem. Soc.* **2000**, *122*, 9977.

(30) Lu, Y.-C.; Chang, C.-W.; Diau, E. W.-G. *J. Chin. Chem. Soc.* **2002**, *49*, 693.

(31) Gundlach, L.; Ernstorfer, R.; Willig, F. *J. Phy. Chem. C* **2007**, *111*, 13586.

(32) Clark, C. C.; Meyer, G. J.; Wei, Q.; Galoppini, E. *J. Phy. Chem. B* **2006**, *110*, 11044.

(33) Perrin, D. D.; Armarego, W. L. F. *Purification of laboratory chemicals*, 3rd ed.; Pergamon Press: Oxford, 1988.

(34) Lu, Y. C.; Diau, E. W.-G.; Rau, H. *J. Phys. Chem. A* **2005**, *109*, 2090.

(35) Ito, S.; Matsui, H.; Okada, K.; Kusano, S.; Kitamura, T.; Wada, Y.; Yanagida, S. *Sol. Energy Mater. Sol. Cells* **2004**, *82*, 421.

JP806777R